RESEARCH ARTICLE

Seasonal Ampacities of 110 kV Power Cables Installed in Various Trenches Surrounded by Two-Layered Native Soil

Dardan Klimenta[1], **Marko Šućurović**[2,*], **Ferdinando Salata**[3] and **Rupali Brahmachary**[4]

[1] Faculty of Technical Sciences, University of Priština in Kosovska Mitrovica, Kosovska Mitrovica RS-38220, Serbia
[2] Faculty of Technical Sciences, University of Kragujevac, Čačak RS-32102, Serbia
[3] Department of Astronautical, Electrical and Energy Engineering, Sapienza University of Rome, Rome IT-00185, Italy
[4] Department of Electrical Engineering, National Institute of Technology Durgapur, Durgapur IN-713209, India

Abstract

In analytical and numerical calculations of the underground cable ampacities in accordance with the relevant IEC standards and the IEC technical report, it is usually assumed that the native soil, cable bedding, and other materials used in and around cable trenches are homogeneous, although this is not the case in reality. This paper, however, assumes that the native soil consists of two horizontal layers with different thermal conductivities. The upper native soil layer includes soil material as well as shrinkage cracks between the ground surface and the horizontal plane where the reference soil temperature is measured, whereas the lower native soil layer includes only soil material below the upper layer, without any porosity. The concept of effective thermal conductivity is applied to the upper layer of native soil. It is also assumed that the effective thermal conductivity of the upper native soil layer in the summer and winter periods corresponds to the most unfavorable summer and most common winter conditions, respectively. In this regard, the aim is to determine the seasonal thermal behavior of three 110 kV power cables installed in trefoil touching formation, directly in two-layered native soil or in four different cable trenches surrounded by the same two-layered native soil. Ampacities are determined analytically in MATLAB, using a standard IEC-based procedure for cables in single-layered native soil, as well as numerically in COMSOL Multiphysics 4.3, using FEM-based steady-state thermal analysis for cables in single- and two-layered native soils. The IEC-based ampacities are used as base values. It is determined that the summer and winter ampacities of the 110 kV cables, compared to the corresponding base ampacities, can be increased by up to 28.46% under the most unfavorable summer conditions and by up to 31.92% under the most common winter conditions, respectively.

Keywords: finite element method (FEM), seasonal ampacity, two-layered native soil, underground power cable.

Submitted: 20 July 2026
Revised: 22 September 2026
Accepted: 24 September 2026
Published: 26 September 2026

Vol. 2, **No.** 3, 2026.
10.62762/TEPNS.2026.878901

***Corresponding author:**
Marko Šućurović
marko.sucurovic@ftn.kg.ac.rs

Citation
Klimenta, D., Šućurović, M., Salata, F., & Brahmachary, R. (2026). Seasonal Ampacities of 110 kV Power Cables Installed in Various Trenches Surrounded by Two-Layered Native Soil. *ICCK Transactions on Electric Power Networks and Systems*, 2(3), 161–174.

1 Introduction

The analytical [1, 2] and finite element method (FEM) [3] procedures adopted by the International Electrotechnical Commission (IEC) for calculating the ampacity of underground power cables still exhibit distinct shortcomings [4, 5] regarding certain fundamental formulas, assumptions, boundary conditions, and the like. Also, they continue to comply with the approximate equations developed by Neher and McGrath [6], which are based on the assumption that the native soil, cable bedding and other materials used in and around cable trenches are homogeneous and possess uniform thermal conductivities. This assumption can be considered appropriate for materials in cable trenches, native soils that are covered by some protective layers [7–10], and deeper (lower) native soil layers in which there are no shrinkage cracks [11, 12]. The reason for this can be found in the fact that the protected and deeper native soil layers are compacted and denser, which is why they are often less porous and retain less moisture [13]. Specifically, droughts during the summer periods lead to the natural shrinkage of native soil surrounding a cable trench and the formation of large shrinkage cracks in it, i.e., to the pronounced effects of shrinkage and crack porosities. These cracks can reach a depth of 1.5 m, and voids due to shrinkage and crack porosities can occupy 27% of the total volume of native soil at depths of up to 1 m [11, 12]. Consequently, the upper native soil layer that includes air- and water-filled voids is non-homogeneous and an effective thermal conductivity must be determined for it [5]. Accordingly, the FEM-based calculations of seasonal (summer or winter) ampacities should be based on the concept of two-layered native soil [5].

The concept of two-layered native soil has been widely used in power engineering for calculating the equivalent resistivity of non-homogeneous soils in the design of grounding grids [14], for modeling underground power cables in two-layer soil environments [15], for calculating the ampacity of underground power cables [7–10], etc. In particular, a significantly larger number of studies address the cable ampacity problems using this or similar concepts. Zones of dried-out soil around underground power cables were first introduced into the cable ampacity calculations in 1965 by Cox and Coates [16]. One and three power cables installed in a trench filled with bedding, protective and backfill materials and surrounded by single-layered native soil were considered in 1979 by Saleeby et al. [17].

A computational domain of width 12.2 m and depth 6.1 m, consisting of an upper protective layer 1.22 m thick, a lower layer of native soil 4.88 m thick, a trench of width 0.61 m and depth 1.22 m, and one or two power cables in the trench, was analyzed in 1992 by Hanna et al. [7]. To the best of our knowledge, this was the first study in which a two-layered native soil was used in the cable ampacity calculation. In the same year, Slaninka and Morgan [18] provided formulas for the external thermal resistance of a power cable installed directly in various two-layered soils. A detailed thermal analysis of one and two power cables laid in a trench filled with two soil layers, protected with one layer and surrounded by single- or two-layered native soil, was carried out in 1993 and 1994 by Hanna et al. [8–10]. In this thermal analysis, the upper layer of the two-layered native soil had a protective role. The external thermal resistances of power cables grouped together within or beneath a horizontal upper layer of soil were calculated in 1994 by Morgan and Slaninka [19]. A system of three underground power cables, situated within a computational domain identical to the one used in [7], was modeled in 1998 by Hanna et al. [20] using the finite difference method. A sensitivity analysis for the thermal performance of three power cables installed in a trench filled with bedding and backfill materials, covered by an asphalt layer, and surrounded by single-layered native soil was conducted in 2007 by Al-Saud et al. [21].

A power cable installed in a trench filled with one bedding and two backfill materials and surrounded by single-layered native soil was analyzed in 2011 by De Lieto Vollaro et al. [22] for the purpose of determining the thermal resistance between the cable and the ground surface. The operation of a 400 kV three-phase cable line inside a conduit surrounded by heterogeneous native soil was simulated in the same year [23]. To investigate the effect of heterogeneous native soil, Mahmoudi et al. [23] divided the native soil into 27 sections with randomly generated numbers for the thermal resistivities of these sections. Experimental validation of the approximate model for determining the thermal resistance between an underground cable and the ground surface proposed earlier by De Lieto Vollaro et al. [24] was performed in 2014 by the same researchers. This experimental validation included cases where the cable trench was filled with layers of materials with different thermal properties and surrounded by single-layered native soil.

An optimal ladder-type soil model for dynamic thermal rating of underground power cables based on a physical discretization of the surrounding soil into a few layers was introduced in 2014 by Diaz-Aguiló et al. [25]. An underground cable line installed in a trench filled with bedding and backfill materials and surrounded by five-layered native soil was analyzed in 2015 by Ocłoń et al. [26] using the FEM. In the same year, the thermal field around an underground power cable was analyzed experimentally and numerically for the cases of different trenches surrounded by single-layered native soil [27]. To investigate the effect of heterogeneous native soil on the ampacity of an underground cable line directly buried in it, the native soil was divided into two sections with different thermal resistivities in 2017 by Duraisamy et al. [28]. However, this division was not made parallel to the ground surface, but vertically with respect to the route of the cable line. In 2020, Nguyen [29] developed a FEM-based steady-state thermal model for the ampacity calculation of a three-phase cable system laid in a trench filled with bedding and backfill materials and surrounded by single-layered native soil. Another system of three single-core power cables laid in flat formation in multi-layered native soil was analyzed in 2021 by Balla et al. [30] using the FEM.

Based on this literature review, it is evident that existing studies, except for the authors' recent study [5], which considered only the most unfavorable summer conditions and cables installed directly in the native soil, do not divide the native soil surrounding a cable trench into two or more layers to account for the effects of shrinkage and crack porosities on the ampacity of underground power cables and heat transferred from the cables to the reference soils. This is identified as a research gap that needs to be filled.

This paper fills the identified research gap by solving five examples involving three 110 kV cables of the type AXLJ 1×1000/190 mm^2 in trefoil touching formation, installed directly in two-layered native soil, as well as in a cable trench (surrounded by two-layered native soil) in four different ways. In this regard, it is assumed that the upper native soil layer contains shrinkage cracks extending to a depth of 1.5 m, while the lower native soil layer does not. Four seasonal base ampacities will be calculated according to the IEC 60287 standards [1, 2], using a procedure implemented in MATLAB. Two additional large-scale (40 m × 21.5 m) and two additional small-scale (10 m × 5 m) computational domains with single-layered native soil will be used for FEM-based recalculations of the same base ampacities (at the continuously permissible conductor temperature of 90 °C of XLPE-insulated cables) in COMSOL Multiphysics 4.3 [31]. The first and second base ampacities correspond to the case where the 110 kV cables are directly laid in single-layered native soil, while the third and fourth base ampacities correspond to the case where the 110 kV cables are laid in a 1.2 m wide and 0.65 m high cable bedding surrounded by single-layered native soil. Then, a series of FEM-based calculations will be carried out using a small-scale computational domain (10 m × 5 m), where the 110 kV cables are de-energized and directly laid in two-layered native soil, assuming that the thermal conductivity of the lower native soil layer is known. These calculations will be performed with the aim of determining the effective thermal conductivity of the upper native soil layer under the most unfavorable summer or most common winter conditions in accordance with [5]. The condition that the temperature of the reference soil at the cable installation depth is equal to the corresponding measured value is used to determine these thermal conductivities [5]. For the most unfavorable summer conditions, the measured reference soil temperature is 20 °C at a depth of 1.5 m, whereas for the most common winter conditions, this temperature is 5 °C at the same depth [32, 33]. In this specific case, the depth reached by shrinkage cracks and the depth at which the reference soil temperature was measured are identical to the depth of the horizontal plane where the 110 kV cables are installed. This coincidence simplifies the calibration of the effective thermal conductivity. In addition, it is assumed that the 110 kV cables operate under balanced three-phase loads. The next series of FEM-based calculations is conducted with the aim of determining the cable ampacities using different small-scale computational domains. The original contributions of this study are as follows: (i) determining the effective thermal conductivity for the upper native soil layer under the most common winter conditions of a temperate-continental climate; (ii) thermal modeling of the upper and lower surfaces of various small-scale computational domains (with a coupled convection-radiation boundary condition and a constant temperature, respectively) for the purpose of calculating the summer and winter cable ampacities; and (iii) calculating the summer and winter ampacities of the considered 110 kV underground cable line for five different installation types, taking into account the effects of shrinkage and crack porosities. The correctness of the FEM-based modeling was verified by means of the results of finite element (FE) mesh independence tests.

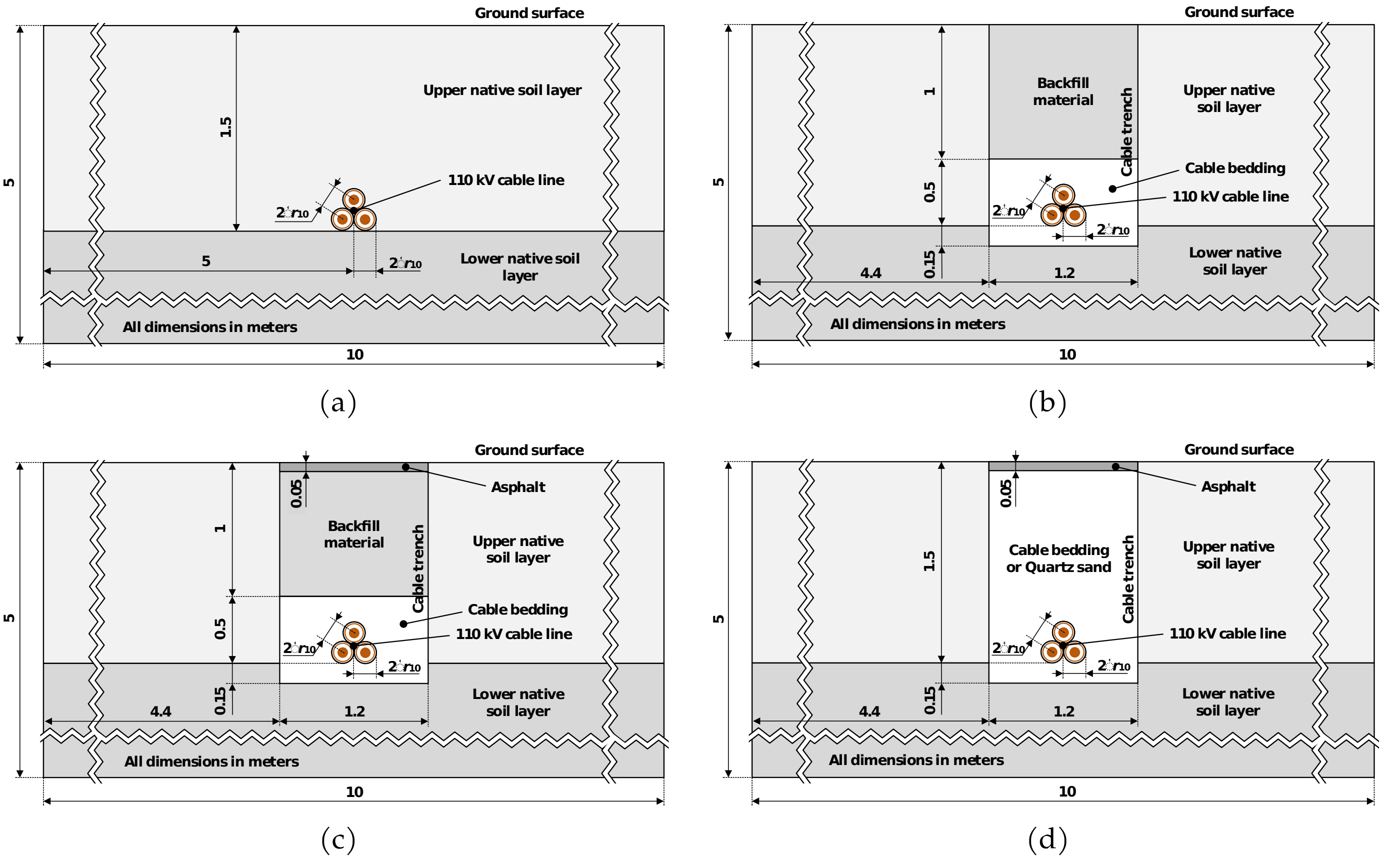

Figure 1. Representation of the small-scale computational domains with the considered 110 kV underground cable line installed (a) directly in two-layered native soil – Case 1; (b) in a trench filled with cable bedding and backfill materials and surrounded by two-layered native soil – Case 2; (c) in a trench filled with cable bedding and backfill materials, covered by an asphalt layer and surrounded by two-layered native soil – Case 3; and (d) in a trench completely filled with cable bedding material or quartz sand, covered by an asphalt layer and surrounded by two-layered native soil – Case 4 or Case 5, respectively.

2 Problem Formulation

To illustrate the coupled effects of shrinkage cracks and different service conditions on the seasonal ampacities of the considered 110 kV underground cable line, the small-scale computational domains in Figures 1a, 1b, 1c and 1d will be considered. The parameter r_{10} appearing in Figure 1 represents the radius of a single 110 kV cable in m. The small-scale computational domains in Figures 1a, 1b and 1c are marked with Case 1, Case 2 and Case 3, respectively. When the trench in Figure 1d is completely filled with cable bedding material, it is Case 4, and when the trench in Figure 1d is completely filled with quartz sand, it is Case 5.

In addition to the small-scale computational domains in Figure 1, four additional computational domains, two large-scale and two small-scale, were also created and used. These four domains consisted of single-layered native soil (moderately dried-out under the most unfavorable summer conditions and in a normal state under the most common winter conditions, see Table 1), adiabatic left, right and lower boundaries, and an isothermal ground surface with a temperature equal to the reference soil temperature measured at the cable installation depth. In one large-scale and one additional small-scale domain, the 110 kV cables are installed directly in single-layered native soil, while in the remaining two additional domains, they are installed in a cable bedding (1.2 m × 0.65 m) surrounded by single-layered native soil. Under the condition that the native soil is single-layered, the first and second additional small-scale domains correspond to the small-scale domains in Figure 1a and 1b, respectively. This is also applicable to the first and second additional large-scale domains if their external dimensions are excluded. The four additional domains and accompanying FEM-based models are created to comply with the appropriate IEC-based analytical procedures [1, 2, 34] and to verify the accuracy of the seasonal base ampacities calculated in accordance with the IEC-based procedures.

The ground surface in the small-scale computational domains in Figure 1 is modeled by the coupling of radiated heat flux, received heat flux and convection boundary conditions. For all the computational domains, both small- and large-scale, the reference soil temperatures measured at a depth of 1.5 m are those given in Table 1 [32, 33]. The small-scale computational domains are created in line with IEC TR 62095 [3]. In the case of the most common winter conditions, the small-scale computational domain in Figure 1a is used for simulations with: (i) de-energized cables and a homogeneous lower native soil layer with a thermal conductivity of 1 W/(K·m) – for adjusting the effective thermal conductivity of the upper native soil layer to winter conditions; and (ii) energized cables and thermal conductivities of the upper and lower native soil layers obtained in the previous step – for determining the corresponding winter FEM-based ampacity. For the most unfavorable summer conditions, the corresponding summer FEM-based ampacity was determined in [5] by applying the small-scale computational domain from Figure 1a and following the same principle.

Each AXLJ 1×1000/190 mm^2 110 kV cable consists of ten cylindrical elements. The radii of these cylindrical elements are listed in Table 2. According to [1, 4, 5], each AXLJ 1×1000/190 mm^2 110 kV cable is modeled by an equivalent design consisting of (i) an aluminum conductor with a radius of $r_1 = 0.0192$ m and a thermal conductivity of $k_1 = 239$ W/(K·m); (ii) an equivalent cross-linked polyethylene (XLPE) insulation layer with an outer radius of $r_5 = 0.03565$ m and a thermal conductivity of $k_5 = 0.286$ W/(K·m); (iii) an equivalent copper screen with an outer radius of $r_8 = 0.03835$ m and a thermal conductivity of $k_8 = 385$ W/(K·m); and (iv) an equivalent high-density polyethylene (HDPE) sheath with an outer radius of $r_{10} = 0.04215$ m and a thermal conductivity of $k_{10} = 0.245$ W/(K·m).

For this equivalent design, the following assumptions are introduced [1, 2, 34]: (i) phase ampacities are mutually equal and balanced; (ii) there is volumetric heat generation in the equivalent XLPE insulation layers amounting to 127.936 W/m^3; and (iii) equivalent copper screens are cross-bonded and there is no heat generation in them. Table 3 lists the seasonal IEC-based values for the external thermal resistance T_4, the ampacity I and volumetric heat generation in the conductors $Q_{v,c}$. The accuracy of the seasonal IEC-based ampacities is verified by means of the additional large- and small-scale domains.

Table 1. The most unfavorable summer and most common winter conditions for underground power cables installed in the temperate-continental climate zone.

Parameter	Most unfavorable summer	Most common winter
Air temperature (°C)	40	5
Solar irradiance (W/m^2)	1000	500
Reference soil temperature at the cable installation depth (°C)	20	5
Reference soil temperature below underground power cables (°C)	8	8
Thermal conductivity of native soil in a normal state (W/(K·m))	1	1
Thermal conductivity of native soil in a moderately dried-out state (W/(K·m))	0.4	0.4

Table 2. Dimensions of the construction elements of the AXLJ 1×1000/190 mm^2 110 kV cable.

Cable construction layer	Outer radius (m)
Aluminum conductor (1000 mm^2) – r_1	0.0192
Semi-conductive XLPE screen – r_2	0.02095
XLPE insulation – r_3	0.03405
Semi-conductive XLPE screen – r_4	0.03505
Semi-conductive PE tapes – r_5	0.03565
Copper screen (190 mm^2) – r_6	0.03755
Semi-conductive PE tapes – r_7	0.03815
Radial water-sealing aluminum layer – r_8	0.03835
Conductive HDPE layer – r_9	0.03855
Outer HDPE sheath – r_{10}	0.04215

The most unfavorable summer and most common winter conditions for underground power cables installed in the temperate-continental zone are listed in Table 1. In addition, for the ground surface in each of the computational domains, radiation properties and convection heat transfer coefficient are $\alpha = 0.6$ – solar absorptivity, $\varepsilon = 0.94$ – thermal emissivity, and $h_c = 12.654$ W/(m^2·K) – convection heat transfer coefficient [4, 5].

Table 3. Summer and winter IEC-based external thermal resistances, ampacities and volumetric heat generation in the conductors of the AXLJ 1×1000/190 mm^2 110 kV cables.

Conductor performance	Cables installed directly in native soil		Cables installed in cable bedding	
	Most unfavorable summer	Most common winter	Most unfavorable summer	Most common winter
Base ampacity label	First	Second	Third	Fourth
External thermal resistance T_4 (K·m/W)	4.285	1.714	2.770	1.498
Seasonal IEC-based ampacity I (A)	593.972	977.162	723.619	1030.799
Seasonal volumetric heat generation $Q_{v,c}$ (W/m^3)	12496.5	33821.3	18547.1	37636.1

3 Steady-State Thermal Modeling

The large- and small-scale two-dimensional non-linear models are analyzed using the FEM, and associated steady-state thermal analyses are governed by the following partial differential equation [4, 5]:

$$\nabla \cdot (-k\nabla T) = Q_v \tag{1}$$

where T is the unknown nodal temperature in K; ∇T is the temperature gradient in K/m; k is the thermal conductivity in W/(K·m); and Q_v is the power of volumetric heat generation in W/m^3. The powers of volumetric heat generation in three aluminum conductors and three equivalent XLPE insulation layers are calculated in accordance with the relevant IEC standards [1, 35] using appropriate formulas and data from [5].

The four additional FEM-based steady-state thermal models with single-layered native soil, two large-scale and two small-scale, are created to comply with IEC 60287-1-1 [1], IEC 60287-2-1 [2], IEC 60287-3-1 [34] and IEC TR 62095 [3]. To implement this, the following boundary conditions are assigned to the external boundaries of the four additional domains: (i) an isothermal Dirichlet boundary condition on the ground surface – an isothermal ground surface with a temperature equal to the reference soil temperature measured at the cable installation depth, i.e.,

$$T = T_{rs} \tag{2}$$

where T is the unknown temperature of the upper boundary (that is, ground surface) in K, and T_{rs} is the reference soil temperature measured at the cable installation depth, or temperature of the ground surface in K; and (ii) an adiabatic Neumann boundary condition on the left, right and lower external boundaries – it is assumed that these boundaries are thermally insulated, i.e.,

$$\vec{n} \cdot (-k\nabla T) = 0 \tag{3}$$

where T is the unknown temperature of the left, right or lower boundary (or domain boundary surface) in K; and $\vec{n}$ is the outwards-oriented normal vector of the adiabatic Neumann boundaries.

The boundaries in each of the five FEM-based steady-state thermal models with two-layered native soil, having external dimensions 10 m × 5 m, are modeled in the following way [5]: (i) a coupling of

$$\vec{n} \cdot (-k\nabla T) = \varepsilon \cdot \sigma_{SB} \cdot \left(T^4 - T_a^4\right) \tag{4}$$

– radiated heat flux,

$$\vec{n} \cdot (-k\nabla T) = -\alpha \cdot Q_{S,s} \tag{5}$$

– received heat flux and

$$\vec{n} \cdot (-k\nabla T) = h_c\,(T - T_a) \tag{6}$$

– convection Robin boundary conditions are assigned to the ground surface, where $\vec{n}$ is the outwards-oriented normal vector of the radiation and Robin boundaries, ε is the thermal emissivity, $\sigma_{SB} = 5.67 \times 10^{-8}$ W/(m^2·K^4) is the Stefan–Boltzmann constant, T_a is the ambient temperature or temperature of air above the ground in K; α is the solar absorptivity, $Q_{S,s}$ is the solar irradiance in W/m^2, h_c is the heat transfer coefficient by convection in W/(m^2·K), while the other parameters and variables were already defined; (ii) an adiabatic Neumann boundary condition (3) is also assigned to the left and right external boundaries; and (iii) an isothermal Dirichlet boundary condition is assigned to the lower external boundary – an isothermal surface with a temperature equal to

Table 4. Summer and winter ampacities of the AXLJ $1\times1000/190$ mm^2 110 kV cables calculated using the relevant IEC-based procedures and FEM-based steady-state thermal models in two different scales.

Conductor performance	Unit	Cables installed directly in native soil		Cables installed in cable bedding	
		Most unfavorable summer	Most common winter	Most unfavorable summer	Most common winter
Base ampacity label	–	First	Second	Third	Fourth
Base ampacity, i.e., seasonal IEC-based ampacity	(A)	593.972	977.162	723.619	1030.799
Seasonal FEM-based ampacity obtained using the corresponding additional large-scale domain	(A)	592.408	973.892	729.519	1027.018
Difference relative to the base ampacity	(%)	-0.263	-0.335	0.815	-0.367
Seasonal FEM-based ampacity obtained using the corresponding additional small-scale domain	(A)	582.586	959.843	714.369	1011.360
Difference relative to the base ampacity	(%)	-1.917	-1.772	-1.278	-1.886

the average temperature of drinking water from groundwater sources in the temperate-continental climate zone, i.e.,

$$T = T'_{rs} \tag{7}$$

where T'_{rs} is the temperature of the reference soil below the underground cable line in K.

4 Results and Discussion

4.1 Verification of FEM-Based Steady-State Thermal Models at a Small Scale

The summer and winter FEM-based ampacities will be compared with the corresponding base ampacities, i.e., the corresponding summer and winter IEC-based values. For the purposes of the comparisons at a large scale, the seasonal FEM-based ampacities were determined using two additional large-scale domains for the case when the boundary conditions at the external surfaces of these domains correspond to the assumptions from the relevant IEC-based procedures (which comply with the approximate equations provided by Neher and McGrath [6]). In addition, for the purposes of the comparisons at a small scale, the seasonal FEM-based ampacities were determined using two additional small-scale domains under the same boundary and other service conditions. In all the additional domains and accompanying FEM-based steady-state thermal models, the native soil is single-layered and has a thermal conductivity of 0.4 W/(K·m) under the most unfavorable summer conditions and 1 W/(K·m) under the most common winter conditions. Also, the thermal conductivity of the cable bedding in some of these models is 1.333 W/(K·m).

Table 4 outlines the summer and winter ampacities of the AXLJ $1\times1000/190$ mm^2 110 kV cables calculated (at a continuously permissible temperature of 90 °C) using the relevant IEC-based procedures and FEM-based steady-state thermal models in two different scales, together with the percentage differences between the seasonal FEM-based ampacities and the corresponding base ampacities.

The percentage differences of the seasonal FEM-based ampacities obtained using the two additional large-scale domains relative to the corresponding base ampacities range between -0.367% and 0.815%. In the case of the two additional small-scale domains, these absolute differences are below 2%, which is acceptable in terms of the required accuracy. Therefore, based on these comparisons, the accuracy of the FEM-based steady-state thermal models at a small scale can be considered verified, and the procedure for determining the unknown effective thermal conductivities can be initiated.

4.2 Effective Thermal Conductivity of the Upper Native Soil Layer

The effective thermal conductivity of the upper native soil layer under the most unfavorable summer conditions is 0.211 W/(K·m), and was determined in [5]. Further, the same procedure from [5] was

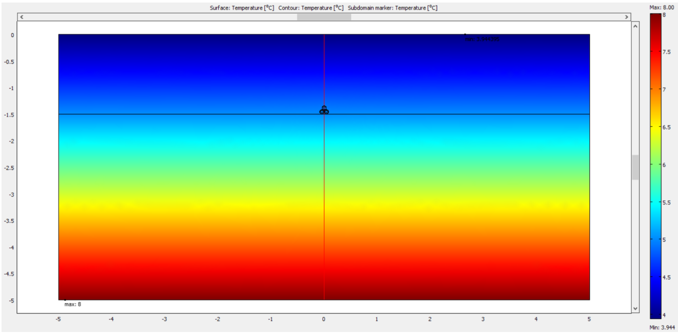

(a)

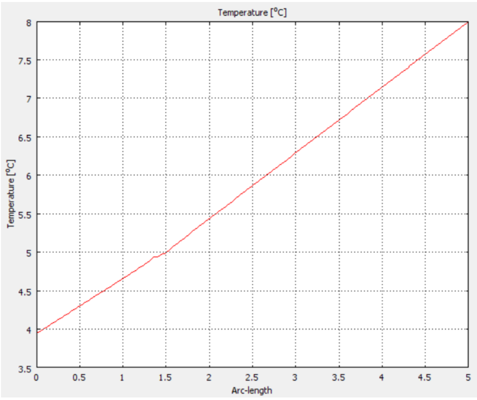

(b)

Figure 2. Final results of simulations with the small-scale computational domain in Figure 1a, generated for de-energized 110 kV cables and the most common winter conditions: (a) spatial temperature distribution; and (b) temperature variation along the vertical axis of symmetry of the computational domain.

repeated, but now for the case of the small-scale computational domain from Figure 1a under the most common winter conditions from Table 1. The final temperature distributions over the domain in Figure 1a and along its vertical axis of symmetry, generated for de-energized 110 kV cables and the most common winter conditions, are shown in Figures 2a and 2b, respectively. The last simulation from this series yielded an effective thermal conductivity of 1.2 W/(K·m) for the upper native soil layer under the most common winter conditions.

Based on Figure 2, the reference soil temperature simulated at the cable installation depth of 1.5 m is equal to the corresponding measured value of 5 °C. This result can be considered physically plausible and realistic. In addition, according to Figure 2, it is obvious that the air above the ground surface thermally affects the native soil layers below the cable installation depth. This agrees with the finding that the air temperature strongly affects the native soil layers up to a depth of 3.6 m [36].

4.3 Seasonal FEM-Based Ampacities of the 110 kV Cable Line Installed Directly in Two-Layered Native Soil

The temperature distributions over the small-scale computational domain in Figure 1a for energized 110 kV cables and the most unfavorable summer conditions from Table 1 were generated and reported in [5] – Case 1 under the most unfavorable summer conditions. Based on [5], the summer FEM-based values for the power of volumetric heat generation in the conductors and the ampacity are: $Q_{v,c} = 14231.4$ W/m^3 and $I = 633.863$ A. The summer FEM-based ampacity is 39.891 A or 6.72% higher than the corresponding summer IEC-based ampacity of 593.972 A from Table 3 [5].

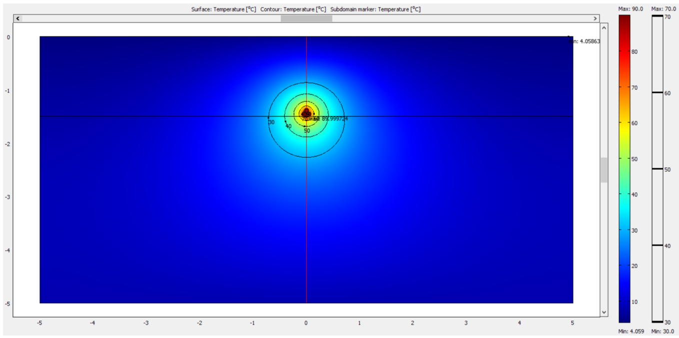

(a)

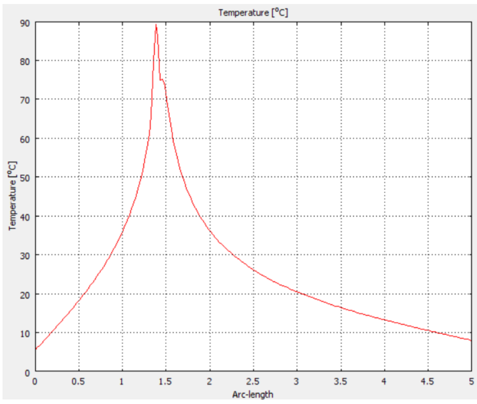

(b)

Figure 3. Final results of simulations with the small-scale computational domain in Figure 1a generated for energized 110 kV cables and the most common winter conditions, i.e., for Case 1 under the most common winter conditions: (a) spatial temperature distribution and isotherms of 30, 40, 50, 60 and 70 °C; and (b) temperature variation along the vertical axis of symmetry of the computational domain.

The temperature distributions over the domain in Figure 1a and along its vertical axis of symmetry, generated for energized 110 kV cables and the most common winter conditions from Table 1, are presented in Figures 3a and 3b, respectively. This heat transfer problem represents Case 1 under the most common winter conditions. In Case 1 under the most common winter conditions, the thermal conductivities of the upper and lower native soil layers are 1.2 W/(K·m) and 1 W/(K·m), respectively. Solving this problem resulted in: $Q_{v,c} = 37703.5$ W/m^3 and $I = 1031.721$ A.

According to Figure 3, the simulated reference soil temperature at the installation depth of 1.5 m is approximately equal to the corresponding measured value. In addition, the winter FEM-based ampacity is 54.559 A or 5.583% higher than the corresponding winter IEC-based ampacity of 977.162 A (from Table 3). Both results are realistic and physically plausible.

4.4 Seasonal FEM-Based Ampacities of the 110 kV Cable Line Installed in Various Trenches Surrounded by Two-Layered Native Soil

The temperature distribution and isotherms of 30, 40, 50, 60 and 70 °C over the small-scale computational domain in Figure 1b, generated for Case 2 under the most unfavorable summer conditions from Table 1, are shown in Figure 4. In Case 2, the thermal conductivities of the upper native soil layer and the backfill material are equal to 0.211 W/(K·m), while the thermal conductivities of the lower native soil layer and the cable bedding are 1 W/(K·m) and 1.333 W/(K·m), respectively. The final results of this series of simulations are: $Q_{v,c} = 21326.5$ W/m^3 and $I = 775.946$ A.

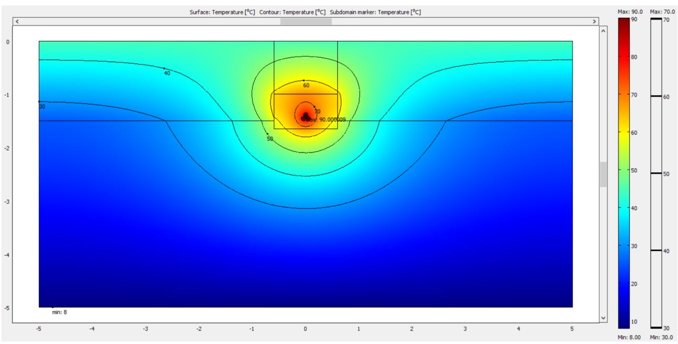

Figure 4. Temperature distribution and isotherms of 30, 40, 50, 60 and 70 °C over the small-scale computational domain in Figure 1b generated for energized 110 kV cables and the most unfavorable summer conditions, i.e., for Case 2 under the most unfavorable summer conditions.

Based on Figure 4, the simulated reference soil temperature at the installation depth of 1.5 m, on the left and right boundaries of the computational domain, is close to the corresponding measured value. Furthermore, the obtained summer FEM-based ampacity is 52.327 A or 7.231% higher than the corresponding summer IEC-based ampacity of 723.619 A from Table 3. Accordingly, the obtained results can be regarded as realistic and physically plausible.

Figure 5 shows the temperature distribution and isotherms of 20, 30, 40, 50, 60 and 70 °C simulated with the small-scale computational domain in Figure 1b. These results are generated for Case 2 under the most common winter conditions from Table 1. In this particular case, the thermal conductivities of the upper native soil layer and the backfill material are equal to 1.2 W/(K·m), while the thermal conductivities of other materials are identical to those from Case 2 under the most unfavorable summer conditions. The final results of these simulations are: $Q_{v,c} = 39941$ W/m^3 and $I = 1061.894$ A.

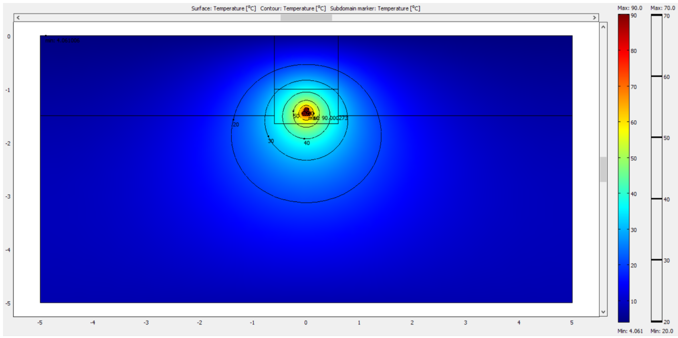

Figure 5. Temperature distribution and isotherms of 20, 30, 40, 50, 60 and 70 °C over the small-scale computational domain in Figure 1b generated for energized 110 kV cables and the most common winter conditions, i.e., for Case 2 under the most common winter conditions.

From Figure 5, it is evident that the simulated and measured reference soil temperatures are close to each other at the installation depth of 1.5 m on the left and right boundaries of the computational domain. Also, the winter FEM-based ampacity is 31.095 A or 3.017% higher than the corresponding winter IEC-based value of 1030.799 A from Table 3. Again, the obtained results can be considered realistic and physically plausible.

The base and FEM-based ampacities for Cases 3–5 and the most unfavorable summer conditions are calculated based on the temperature distributions generated over the small-scale computational domains in Figure 1c and 1d. These summer ampacities and the base and FEM-based ampacities obtained for Cases 1 and 2 under the most unfavorable summer conditions are shown together in Figure 6. For Cases 3–5 under the most unfavorable summer conditions, the thermal conductivities were as follows: 0.211 W/(K·m) – for the upper native soil layer, 1 W/(K·m) – for the lower native soil layer, 1.333 W/(K·m) – for the cable bedding, 5 W/(K·m) – for the quartz sand, 1 W/(K·m) – for the backfill material, and 1.2 W/(K·m) – for the asphalt layer.

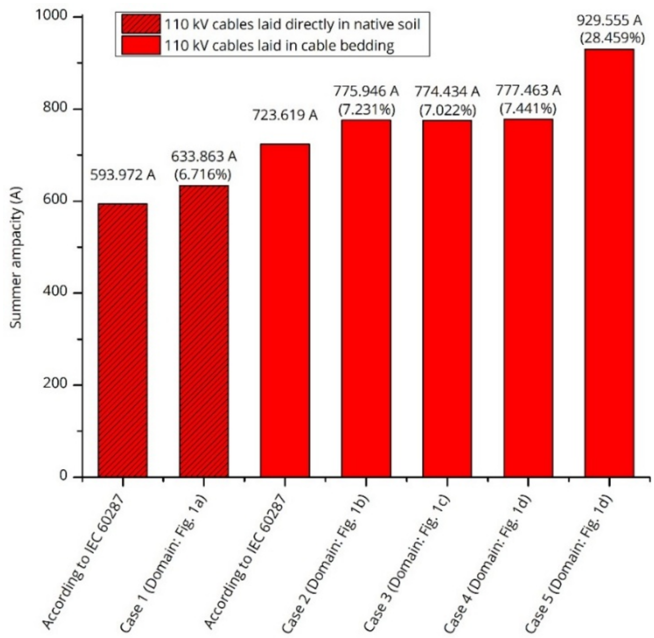

Figure 6. Base and FEM-based ampacities obtained using the computational domains in Figure 1 for Cases 1–5 and the most unfavorable summer conditions.

Figure 7 shows the base and FEM-based ampacities calculated for Cases 3–5 and the most common winter conditions. The winter FEM-based ampacities are calculated based on the temperature distributions generated over the computational domains in Figure 1c and 1d. Figure 7 also shows the base and FEM-based ampacities obtained for Cases 1 and 2 under the most common winter conditions. The thermal conductivity values of the materials used in these simulations are provided in the description of Figure 6, except that the effective thermal conductivity of the upper native soil layer is 1.2 W/(K·m) under the most common winter conditions.

Based on Figures 6 and 7, it is evident that all the base ampacities (i.e., all the seasonal IEC-based ampacities) were calculated with a certain safety margin and are independent of the shrinkage cracks contained within the upper native soil layer. Various types of underground cable installations increase their ampacities relative to the corresponding base values. The greatest increases in seasonal ampacity are achieved when the cable trench is completely filled with quartz sand. They amount to 28.459% for the most unfavorable summer conditions and 31.917% for the most common winter conditions. For Cases 1–4, the increases in seasonal ampacity are more pronounced under the most unfavorable summer conditions

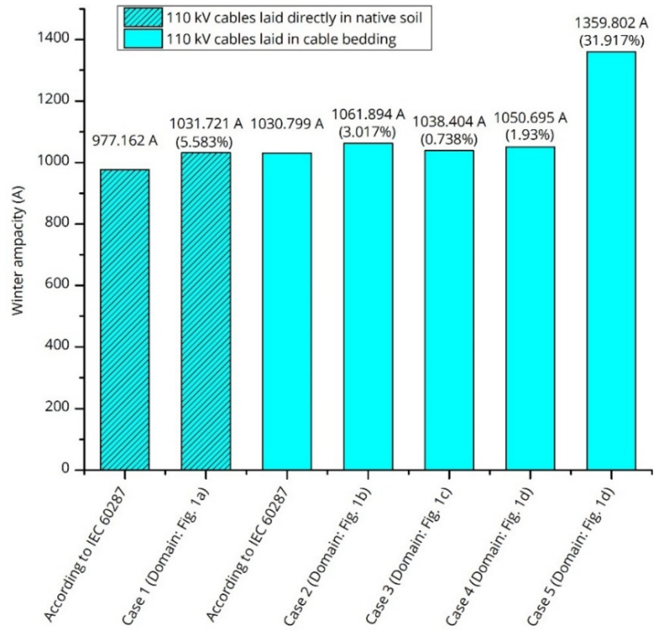

Figure 7. Base and FEM-based ampacities obtained using the computational domains in Figure 1 for Cases 1–5 and the most common winter conditions.

(6.716–7.441% versus 0.738–5.583%), whereas for Case 5 the increase is larger under the most common winter conditions. Given that Case 5 yielded the greatest increase in cable ampacity compared to the corresponding IEC-based value, the question of economic feasibility can be raised for the type of installation with quartz sand. The economic viability of this type of installation was previously examined, and the results of that analysis can be found in [37].

4.5 Finite Element Mesh Independence Tests

The results of FE mesh independence tests conducted using the FEM-based steady-state thermal models whose geometries are shown in Figure 1 for the most unfavorable summer conditions are presented in Table 5. The results corresponding to Case 1 are identical to those reported in [5]. The FE mesh independence tests included three different densities of FE meshes, and the maximum conductor temperatures were tracked. For each model considered, the differences between every two maximum conductor temperatures were less than 0.03 °C. Identical FE mesh independence tests were conducted for Cases 1–5 and the most common winter conditions. In this particular case, the temperature differences were less than 0.007 °C. Therefore, it is obvious that the maximum conductor temperatures and associated seasonal FEM-based ampacities were not affected by the different FE mesh densities.

Table 5. Results of FE mesh independence tests conducted using the considered FEM-based thermal models for the most unfavorable summer conditions.

Case / Domain	FE mesh	Number of nodes	Number of finite elements	Maximum conductor temperature (°C)	Conductor temperature deviation (°C)
Case 1 / Figure 1a	Default generation	2717	5375	90.000306	–
	After the first refinement	10808	21500	90.002912	+0.002606
	After the second refinement	43115	86000	90.003027	+0.002721
Case 2 / Figure 1b	Default generation	2638	5222	90.000009	–
	After the first refinement	10497	20888	90.013834	+0.013825
	After the second refinement	41881	83552	90.017735	+0.017726
Case 3 / Figure 1c	Default generation	2808	5537	89.999512	–
	After the first refinement	11152	22148	90.013132	+0.013620
	After the second refinement	44451	88592	90.017210	+0.017698
Case 4 / Figure 1d	Default generation	2828	5577	90.000042	–
	After the first refinement	11232	22308	90.014234	+0.014192
	After the second refinement	44771	89232	90.018497	+0.018455
Case 5 / Figure 1d	Default generation	2828	5577	89.999993	–
	After the first refinement	11232	22308	90.021618	+0.021625
	After the second refinement	44771	89232	90.028603	+0.028610

5 Conclusion

The general conclusions that can be drawn based on the results of this study are:

- It was shown that the seasonal thermal effects of shrinkage cracks on the thermal conductivity of the upper native soil layer can be modeled using the concept of effective thermal conductivity. In this regard, the effective thermal conductivity of the upper native soil layer, affected by shrinkage cracks up to the cable installation depth, can be 0.211 W/(K·m) under the most unfavorable summer conditions and 1.2 W/(K·m) under the most common winter conditions.

- Thermal modeling of the ground surface with a coupled convection-radiation boundary condition and the reference soil below underground power cables with a constant temperature provided realistic and physically plausible seasonal ampacities for all the considered types of underground cable installations.

- It was found that there is a certain safety margin in the IEC 60287-based calculations of underground cable ampacities regarding the thermal effects of shrinkage cracks.

- It was shown that the seasonal ampacities of a 110 kV underground cable line, compared to the corresponding base ampacities, can be increased by up to 28.46% under the most unfavorable summer conditions and 31.92% under the most common winter conditions when its trench is completely filled with quartz sand. This is a consequence of the reduced external thermal resistance between the underground power cables and the ground surface, owing to the high thermal conductivity of the quartz sand that fills the whole trench, combined with the heat dissipation from the ground surface modeled by a coupled convection-radiation boundary condition.

- The accuracy of the FEM-based steady-state thermal models used was successfully verified using additional FEM-based models created in accordance with IEC 60287 and IEC TR 62095, FE mesh independence tests, and reference soil temperatures measured at the cable installation depth.

Although the accuracy of the proposed FEM-based models was verified against the relevant IEC-based calculations and FE mesh independence tests, their full experimental validation against field-measured ampacities of underground cable lines remains open and should be addressed in future work. In addition, future research should apply the proposed approach to calculating the ampacities of low-voltage underground cables laid in shallow trenches and at various depths. Furthermore, the applicability of the proposed approach should be considered for cases where low-voltage underground cables are installed beneath cool or photovoltaic pavements.

Data Availability Statement

Data will be made available on request.

Funding

This work was supported by the Government of the Republic of Serbia under Grant No. 451-03-34/2026-03/200155 and Grant No. 451-03-34/2026-03/200132.

Conflicts of Interest

Dardan Klimenta served as an Editor-in-Chief, and Ferdinando Salata served as an Associate Editor of the *ICCK Transactions on Electric Power Networks and Systems* at the time of manuscript submission. To ensure the integrity of the peer-review process, neither Dardan Klimenta nor Ferdinando Salata was involved in the editorial handling, peer review, or decision-making process for this manuscript, which was handled independently by another editor. The remaining authors declare no conflicts of interest.

AI Use Statement

The authors declare that no generative AI was used in the preparation of this manuscript.

Ethical Approval and Consent to Participate

Not applicable.

References

[1] International Electrotechnical Commission. (2023). *Electric cables - Calculation of the current rating - Part 1-1: Current rating equations (100 % load factor) and calculation of losses - General* (Standard IEC 60287-1-1:2023 CMV). IEC. Retrieved from https://webstore.iec.ch/en/publication/85666

[2] International Electrotechnical Commission. (2023). *Electric cables - Calculation of the current rating - Part 2-1: Thermal resistance - Calculation of thermal resistance* (Standard IEC 60287-2-1:2023 CMV). IEC. Retrieved from https://webstore.iec.ch/en/publication/85669

[3] International Electrotechnical Commission. (2003). *Electric cables - Calculations for current ratings - Finite element method* (Technical Report IEC TR 62095:2003). IEC. Retrieved from https://webstore.iec.ch/en/publication/6455

[4] Klimenta, D., Šućurović, M., & Tasić, D. (2025). Amendments to some IEC TR 62095 recommendations for underground single-core power cables in trefoil formation. *ICCK Transactions on Electric Power Networks and Systems, 1*(1), 38-49. [CrossRef]

[5] Klimenta, D., Šućurović, M., & Tasić, D. (2026). Thermal modeling of the ground surface for the purpose of calculating the current-carrying capacity of underground cable lines using the FEM. *ICCK Transactions on Electric Power Networks and Systems, 2*(1), 47-57. [CrossRef]

[6] Neher, J. H., & McGrath, M. H. (1957). The calculation of the temperature rise and load capability of cable systems. *Transactions of the American Institute of Electrical Engineers. Part III: Power Apparatus and Systems, 76*, 752-772. [CrossRef]

[7] Hanna, M. A., Chikhani, A. Y., & Salama, M. M. A. (1992, August). Modelling of underground cable systems in non-homogeneous soils. In [1992] *Proceedings of the 35th Midwest Symposium on Circuits and Systems* (pp. 381-384). IEEE. [CrossRef]

[8] Hanna, M. A., Chikhani, A. Y., & Salama, M. M. A. (1993). Thermal analysis of power cables in multi-layered soil - Part 1: Theoretical model. *IEEE Transactions on Power Delivery, 8*(3), 761-771. [CrossRef]

[9] Hanna, M. A., Chikhani, A. Y., & Salama, M. M. A. (1993). Thermal analysis of power cables in multi-layered soil - Part 2: Practical considerations. *IEEE Transactions on Power Delivery, 8*(3), 772-778. [CrossRef]

[10] Hanna, M. A., Chikhani, A. Y., & Salama, M. M. A. (1994). Thermal analysis of power cables in multi-layered soil - Part 3: Case of two cables in a trench. *IEEE Transactions on Power Delivery*, 9(1), 572-578. [CrossRef]

[11] Ackerson, J. P., McInnes, K. J., Morgan, C. L., & Everett, M. E. (2017). Measuring crack porosity using three-dimensional electrical resistivity tomography. *Soil Science Society of America Journal, 81*(5), 1025-1035. [CrossRef]

[12] Bagnall, D. K., Crespo Gutierrez, P. M., Yimam, Y. T., Morgan, C. L., Neely, H. L., & Ackerson, J. P. (2018). Effect of air-and water-filled voids on neutron moisture meter measurements of clay soil. *Vadose Zone Journal, 17*(1), 1-9. [CrossRef]

[13] Khumalo, N. Q., Naidoo, R. M., Mbungu, N. T., & Bansal, R. C. (2025). A Critical Assessment of Cable Rating Methods Under Soil Drying Out Conditions. *International Transactions on Electrical Energy Systems, 2025*(1), 5946564. [CrossRef]

[14] Thapar, B., & Gerez, V. (1995). Equivalent resistivity of non-uniform soil for grounding grid design. *IEEE Transactions on Power Delivery, 10*(2), 759-767. [CrossRef]

[15] Mabrouki, H., Debel, N., Bouallegue, A., & Hadj Abdallah, H. (2014, March 25-27). Modeling of an underground cable fled in two-layer soil. In *2014 First International Conference on Green Energy (ICGE 2014)* (pp. 144-151). IEEE. [CrossRef]

[16] Cox, H. N., & Coates, R. (1965, December). Thermal analysis of power cables in soils of temperature-responsive thermal resistivity. In *Proceedings of the Institution of Electrical Engineers* (Vol. 112, No. 12, pp. 2275-2283). IEE. [CrossRef]

[17] Saleeby, K. E., Black, W. Z., & Hartley, J. G. (1979). Effective thermal resistivity for power cables buried in thermal backfill. *IEEE Transactions on Power Apparatus and Systems, PAS-98*(6), 2201-2214. [CrossRef]

[18] Slaninka, P., & Morgan, V. T. (1992). External thermal resistance of power cable in nonuniform soil. *IEE Proceedings A (Science, Measurement and Technology), 139*(3), 117-124. [CrossRef]

[19] Morgan, V. T., & Slaninka, P. (1994). The external thermal resistance of power cables in a group buried in non-uniform soil. *Electric power systems research, 29*(1), 35-42. [CrossRef]

[20] Hanna, M. A., Chikhani, A. Y., & Salama, M. M. A. (1998). Thermal analysis of power cable systems in a trench in multi-layered soil. *IEEE transactions on power delivery, 13*(2), 304-309. [CrossRef]

[21] Al-Saud, M. S., El-Kady, M. A., & Findlay, R. D. (2007, April). Advanced thermal field sensitivity analysis of power cables. In *2007 Canadian Conference on Electrical and Computer Engineering* (pp. 133-136). IEEE. [CrossRef]

[22] de Lieto Vollaro, R., Fontana, L., & Vallati, A. (2011). Thermal analysis of underground electrical power cables buried in non-homogeneous soils. *Applied Thermal Engineering, 31*(5), 772-778. [CrossRef]

[23] Mahmoudi, A., Kahourzade, S., & Lee, D. S. (2011, June). Cable ampacity calculation in heterogenous soil using finite element analysis. In *2011 5th International Power Engineering and Optimization Conference* (pp. 416-421). IEEE. [CrossRef]

[24] de Lieto Vollaro, R., Fontana, L., & Vallati, A. (2014). Experimental study of thermal field deriving from an underground electrical power cable buried in non-homogeneous soils. *Applied thermal engineering, 62*(2), 390-397. [CrossRef]

[25] Diaz-Aguiló, M., De León, F., Jazebi, S., & Terracciano, M. (2014). Ladder-type soil model for dynamic thermal rating of underground power cables. *IEEE Power and Energy Technology Systems Journal, 1*, 21-30. [CrossRef]

[26] Ocłoń, P., Cisek, P., Pilarczyk, M., & Taler, D. (2015). Numerical simulation of heat dissipation processes in underground power cable system situated in thermal backfill and buried in a multilayered soil. *Energy Conversion and Management, 95*, 352-370. [CrossRef]

[27] Salata, F., De Lieto Vollaro, A., & De Lieto Vollaro, R. (2015). A model for the evaluation of heat loss from underground cables in non-uniform soil to optimize the system design. *Thermal Science, 19*(2), 461-474. [CrossRef]

[28] Duraisamy, N., Gooi, H. B., & Ukil, A. (2017, October 29-November 1). Modeling and analysis of HV cable ampacity for power flow optimization. In *Proceedings of IECON 2017 - 43rd Annual Conference of the IEEE Industrial Electronics Society* (pp. 1-5). IEEE. [CrossRef]

[29] Nguyen, N.-K. (2020, August 18-21). Numerical model of the external thermal resistance of underground cables buried in the multi-layers soil for ampacity calculation. In *2020 4th International Conference on Smart Grid and Smart Cities (ICSGSC 2020)* (pp. 57-63). IEEE. [CrossRef]

[30] Balla, S. J., Walker, J. J., & Kyere, I. K. (2021, November). Application of finite element method to compare the installation requirements in a buried cable according to IEC60287 standards. In *IET Conference Proceedings CP787* (Vol. 2021, No. 15, pp. 907-911). Stevenage, UK: The Institution of Engineering and Technology. [CrossRef]

[31] COMSOL AB. (2012). *COMSOL Multiphysics User's Guide* (Version 4.3). COMSOL AB, Stockholm, Sweden. Retrieved from https://doc.comsol.com/

[32] Sredojević, M. R., Naumov, R. M., Popović, D. P., & Simić, M. D. (1997, June). Long term investigation of thermal behaviour of 110 kV underground transmission lines in the Belgrade area. In *14th International Conference and Exhibition on Electricity Distribution (CIRED 1997), Part 1: Contributions* (IEE Conf. Publ. No. 438, Vol. 3, pp. 44-1). IET. [CrossRef]

[33] Sredojević, M. R., Popović, D. P., & Simić, M. D. (1999, August). Permissible current rating of the investigated 110 kV underground cable line. In *PowerTech Budapest 99. Abstract Records* (Cat. No. 99EX376) (p. 218). IEEE. [CrossRef]

[34] International Electrotechnical Commission. (2017). *Electric cables - Calculation of the current rating - Part 3-1: Operating conditions - Site reference conditions* (Standard IEC 60287-3-1:2017 RLV). IEC. Retrieved from https://webstore.iec.ch/en/publication/60845

[35] International Electrotechnical Commission. (2023). *Conductors of insulated cables* (Standard IEC 60228:2023 CMV). IEC. Retrieved from https://webstore.iec.ch/en/publication/90329

[36] Kim, Y.-S., Cong, H. N., Dinh, B. H., & Kim, H.-K. (2025). Effect of ambient air and ground temperatures on heat transfer in underground power cable system buried in newly developed cable bedding material. *Geothermics, 125*, 103151. [CrossRef]

[37] Klimenta, D., Jevtić, M., Andriukaitis, D., & Mijailović,

V. (2021). Increasing the transmission performance of a conventional 110 kV cable line by combining a hydronic concrete pavement system with photovoltaic floor tiles. *Electrical Engineering, 103*(3), 1401-1415. [CrossRef]

Dardan Klimenta was born in Serbia, in 1975. He graduated from the Faculty of Electrical Engineering, University of Priština, in 1998. Also, he received his postgraduate M.Sc. and Ph.D. in 2001 and 2007, respectively, from the Faculty of Electrical Engineering, University of Belgrade. His main research interests include electrical power cable engineering, renewable energy sources, electric power system components, heat transfer, optimization methods, FEM and FEA. Currently, he is a Full Professor with the Faculty of Technical Sciences, University of Priština in Kosovska Mitrovica. (Email: dardan.klimenta@pr.ac.rs)

Marko Šućurović was born in Serbia, in 1988. He received his B.Sc. and M.Sc. in 2011 and 2012, respectively, from the Faculty of Technical Sciences in Čačak, University of Kragujevac. Also, he is a Ph.D. student at the Faculty of Electronic Engineering, University of Niš. His main research interests include electrical power cable engineering, renewable energy sources, electric power system components, heat transfer, FEM and FEA. Currently, he is a Teaching and Research Assistant with the Faculty of Technical Sciences in Čačak, University of Kragujevac. (Email: marko.sucurovic@ftn.kg.ac.rs)

Ferdinando Salata was born in Italy in 1977. He graduated in Mechanical Engineering with a specialization in Energy from Sapienza University of Rome in 2003, where he also earned his PhD in Technical Physics in 2008. He is currently an Associate Professor at Sapienza University of Rome in the Department of Astronautical, Electrical and Energy Engineering (DIAEE). Since 2017, he has been a member of the Academic Board of the PhD program in Energy and Environment. His main research interests include urban microclimate modeling, urban heat island mitigation, outdoor and indoor thermo-hygrometric comfort, building energy optimization via genetic algorithms and multi-objective design, the impact of global warming on building energy demand, as well as the sustainability of advanced lighting systems, applied acoustics and heat transfer. (Email: ferdinando.salata@uniroma1.it)

Rupali Brahmachary was born in India, in 1997. She received her B.Tech. degree in Electrical Engineering from Techno India University, West Bengal, in 2018, and her M.Tech. degree in Power Systems Engineering from the National Institute of Technology Nagaland in 2020. She received her Ph.D. degree from the National Institute of Technology Durgapur in 2026. Her main research interests include electric vehicles, demand-side management, distribution network planning and optimization, machine learning-based load forecasting, power quality, and renewable energy integration. She is currently working as a Project Associate-II in the Department of Electrical Engineering, National Institute of Technology Durgapur, India. (Email: brahmachary.rupali29@gmail.com)